Title

Ultrafine Particle Exposure Reveals the Importance of FOXO1/Notch Activation Complex for Vascular Regeneration.

Journal

Antioxidants & redox signaling, 28(13)

ISSN

1523-0864

Authors

Baek, Kyung In
Packard, René R Sevag
Hsu, Jeffrey J
et al.

Publication Date

2018-05-01

DOI

10.1089/ars.2017.7166

Peer reviewed

ANTIOXIDANTS & REDOX SIGNALING
Volume 28, Number 13, 2018

DOI: 10.1089/ars.2017.7166

Discoveries

ORIGINAL RESEARCH COMMUNICATION

Ultrafine Particle Exposure Reveals the Importance of FOXO1/Notch Activation Complex for Vascular Regeneration

Kyung In Baek,[1] René R. Sevag Packard,[2] Jeffrey J. Hsu,[2] Arian Saffari,[3] Zhao Ma,[1] Anh Phuong Luu,[2] Andrew Pietersen,[1] Hilary Yen,[1] Bin Ren,[4,5] Yichen Ding,[2] Constantinos Sioutas,[3] Rongsong Li,[2] and Tzung K. Hsiai[1,2,6]

Abstract

Aims: Redox active ultrafine particles (UFP, $d < 0.2$ μm) promote vascular oxidative stress and atherosclerosis. Notch signaling is intimately involved in vascular homeostasis, in which forkhead box O1 (FOXO1) acts as a co-activator of the Notch activation complex. We elucidated the importance of FOXO1/Notch transcriptional activation complex to restore vascular regeneration after UFP exposure.

Results: In a zebrafish model of tail injury and repair, transgenic *Tg(fli1:GFP)* embryos developed vascular regeneration at 3 days post amputation (dpa), whereas UFP exposure impaired regeneration ($p < 0.05$, $n = 20$ for control, $n = 28$ for UFP). UFP dose dependently reduced Notch reporter activity and Notch signaling-related genes (Dll4, JAG1, JAG2, Notch1b, Hey2, Hes1; $p < 0.05$, $n = 3$). In the transgenic *Tg(tp1:GFP; flk1:mCherry)* embryos, UFP attenuated endothelial Notch activity at the amputation site ($p < 0.05$ *vs.* wild type [WT], $n = 20$). A disintegrin and metalloproteinase domain-containing protein 10 (ADAM10) inhibitor or dominant negative (DN)-*Notch1b* messenger RNA (mRNA) disrupted the vascular network, whereas notch intracellular cytoplasmic domain (*NICD*) mRNA restored the vascular network ($p < 0.05$ *vs.* WT, $n = 20$). UFP reduced FOXO1 expression, but not Master-mind like 1 (MAML1) or NICD ($p < 0.05$, $n = 3$). Immunoprecipitation and immunofluorescence demonstrated that UFP attenuated FOXO1-mediated NICD pull-down and FOXO1/NICD co-localization, respectively ($p < 0.05$, $n = 3$). Although FOXO1 morpholino oligonucleotides (MOs) attenuated Notch activity, *FOXO1* mRNA reversed UFP-mediated reduction in Notch activity to restore vascular regeneration and blood flow ($p < 0.05$ *vs.* WT, $n = 5$).

Innovation and Conclusion: Our findings indicate the importance of the FOXO1/Notch activation complex to restore vascular regeneration after exposure to the redox active UFP. *Antioxid. Redox Signal.* 28, 1209–1223.

Keywords: ultrafine particles, UFP, Notch signaling, FOXO1, tail amputation, vascular repair

Introduction

VASCULAR REGENERATION INVOLVES complex signaling pathways, and exposure to ambient particulate matter ($PM_{2.5}$, $d < 2.5$ μm) is an emerging epigenetic factor to impair vascular regeneration (24, 41). Although $PM_{2.5}$ in air pollution significantly contributes to cancer, cardiovascular, and respiratory diseases (9, 10, 15, 52), recent epidemiological studies indicated an increased risk of cardiovascular defects during development (12, 20). Ultrafine particles (UFP,

[1]Department of Bioengineering, University of California, Los Angeles, Los Angeles, California.
[2]Division of Cardiology, Department of Medicine, University of California, Los Angeles, Los Angeles, California.
[3]Department of Civil and Environmental Engineering, University of Southern California, Los Angeles, California.
[4]Division of Hematology and Oncology, Medical College of Wisconsin, Milwaukee, Wisconsin.
[5]Blood Research Institute, Blood Center of Wisconsin, Milwaukee, Wisconsin.
[6]Research Services, Veteran Affairs Greater Los Angeles Healthcare System, Los Angeles, California.

Innovation

Ambient ultrafine particles suppress forkhead box O-subfamily (FOXO1) as an important co-activator with notch intracellular cytoplasmic domain (NICD) to impair vascular regeneration.

diameter <0.2 μm) are a highly redox-active sub-fraction of $PM_{2.5}$ that is rich in reactive organic chemicals (55) and transition metals (9, 38, 43, 66). UFP exposure activates JNK to produce reactive oxygen species, and it induces NF-κB-mediated inflammatory responses to initiate atherosclerosis and vascular calcification (2, 8, 31, 32, 43, 50, 66). However, the mechanism whereby exposure to ambient UFP impairs vascular regeneration remains unexplored.

The Notch signaling pathway is an evolutionarily conserved intercellular signaling pathway that is critical in cell-fate specification and embryonic development (4, 14, 22, 27, 48, 57). On ligand binding, the Notch receptor undergoes proteolytic cleavages to release notch intracellular cytoplasmic domain (NICD). After translocation to the nuclei, NICD forms a transcriptional activation complex consisting of recombination signal-binding protein for immunoglobulin J region (Rbp-Jκ), suppressor of hairless, Lag-1 (CSL), and master-mind like (MAML) to induce Notch target genes (6).

The Forkhead box O-subfamily (FOXO) protein is a transcription factor that regulates hormonal control, cellular metabolism, and differentiation (1). Analogous to Notch signaling in cell fate and vascular maturation, FOXO1 (*FKHR*), the dominant isoform of the FOXO, is essential for vascular growth. Conditional deletion of FOXO1 results in abnormal sprout formation and vascular migration, resulting in a hyperplastic vascular network; whereas constitutively active FOXO1 suppresses vascular expansion, resulting in a sparse vascular network (62). Endothelial FOXO1 physically interacts with canonical Notch signaling by binding to CSL, enhancing co-repressor clearance to promote Notch signaling (26). FOXO1 ablation recapitulates the Notch1 knockout phenotype, whereas the FOXO1 interaction with NICD promotes Notch1 activation in vascular, muscular, and neuronal differentiation (26).

In this context, we assessed whether exposure to ambient UFP inhibits Notch signaling *via* FOXO1/Notch activation complex to impair vascular regeneration. After tail amputation in embryonic zebrafish, vascular regeneration occurred; whereas UFP exposure attenuated Notch activity and impaired regeneration. UFP further down-regulated FOXO1 expression, resulting in reduced FOXO1 and NICD co-localization. Although rescue with *NICD* messenger RNA (mRNA) partially restored Notch activity, rescue with *FOXO1* mRNA reversed UFP-mediated reduction in Notch activity, leading to restored vascular network and blood flow to the amputated site. Thus, the redox-active UFP down-regulates FOXO1-mediated Notch signaling, revealing the essential role of FOXO1/Notch activation complex in vascular regeneration.

Results

UFP exposure impaired vascular regeneration

To assess the effects of UFP on vascular regeneration, we used the transgenic *Tg(fli1:GFP)* zebrafish embryos to visualize the vascular endothelium in response to tail amputation at 3 days post-fertilization (dpf) (Fig. 1A, B). Embryos in the control group developed a complete loop formation connecting the dorsal aorta (DA) with the dorsal longitudinal anastomotic vessel (DLAV) at 3 days post-amputation (dpa) (Fig. 1C), accompanied with restored blood flow to the amputated site (Supplementary Video S1A; Supplementary Data are available online at www.liebertpub.com/ars); whereas UFP-exposed embryos developed a disrupted vascular network with aberrant blood flow (Fig. 1D) (Supplementary Video S1B). Impaired vascular regeneration was seen in 77% of the UFP-exposed embryos as compared with 20% of the wild type (WT) embryos ($*p < 0.05$, $n = 20$ for WT, $n = 28$ for UFP) (Fig. 1E). As a corollary to the zebrafish model of vascular endothelial injury and regeneration, UFP inhibited both endothelial cell migration and tube formation (Supplementary Fig. S2). Thus, UFP exposure impaired vascular repair.

UFP exposure down-regulated Notch-related genes

To assess Notch signaling in response to UFP exposure, we used the pJH26 Notch reporter. UFP significantly reduced Notch activity in human aortic endothelial cells (HAECs) in a dose-dependent manner ($*p < 0.05$ *vs.* control, $n = 3$) (Fig. 2A), accompanied with down-regulation of Notch signaling-related genes, including Notch ligand *Dll4* and Notch target *Hes1*, in a dose- and time-dependent manner ($*p < 0.05$ *vs.* control, $n = 3$) (Fig. 2B, C). In the zebrafish embryos, UFP exposure also down-regulated Notch signaling-related genes, including Notch ligands (*JAG1* and *JAG2*), the Notch receptor (*Notch1b*), and Notch targets (*Hey2* and *Hes1*) ($*p < 0.05$ *vs.* control, $n = 3$) (Fig. 2D). The UFP-mediated attenuation in Notch signaling was corroborated by a disintegrin and metalloproteinase domain-containing protein 10 (ADAM10) inhibitor (GI254023X) that inhibits Notch receptor activation (Fig. 2D). Thus, UFP inhibited Notch activity and down-regulated Notch-related mRNA expression in both HAEC and zebrafish embryos.

UFP-attenuated Notch signaling impaired vascular regeneration

We further performed gain- and loss-of-function analyses to validate Notch signaling-mediated vascular regeneration in the transgenic *Tg(fli1:GFP)* embryos. Similar to the effects of UFP, ADAM10 inhibitor, GI254023X, impaired vascular regeneration after tail amputation ($*p < 0.05$, $n = 20$) (Fig. 3A, B). However, rescue with *NICD* mRNA attenuated the proportion of embryos with ADAM10 inhibitor- and UFP-impaired vascular regeneration from 65% to 31% and from 80% to 31%, respectively ($*p < 0.05$, $n = 20$) (Fig. 3C). To further assess whether the reduction in Notch signaling impairs vascular regeneration, we constructed a dominant negative *Notch 1b* (DN-*Notch1b*) mRNA that inhibits 96% of Notch signaling (Supplementary Fig. S3). Seventy five percent of embryos injected with DN-*Notch1b* mRNA developed abnormal vascular regeneration and exhibited embryonic lethality ($*p < 0.05$, $n = 20$), which was reduced to 50% by *NICD* mRNA rescue (Fig. 3C). In agreement with DN-*Notch1b* mRNA, UFP exposure during embryogenesis retarded development and promoted embryonic lethality (Supplementary Fig. S5). Hence, UFP-attenuated Notch signaling is implicated in impaired vascular regeneration.

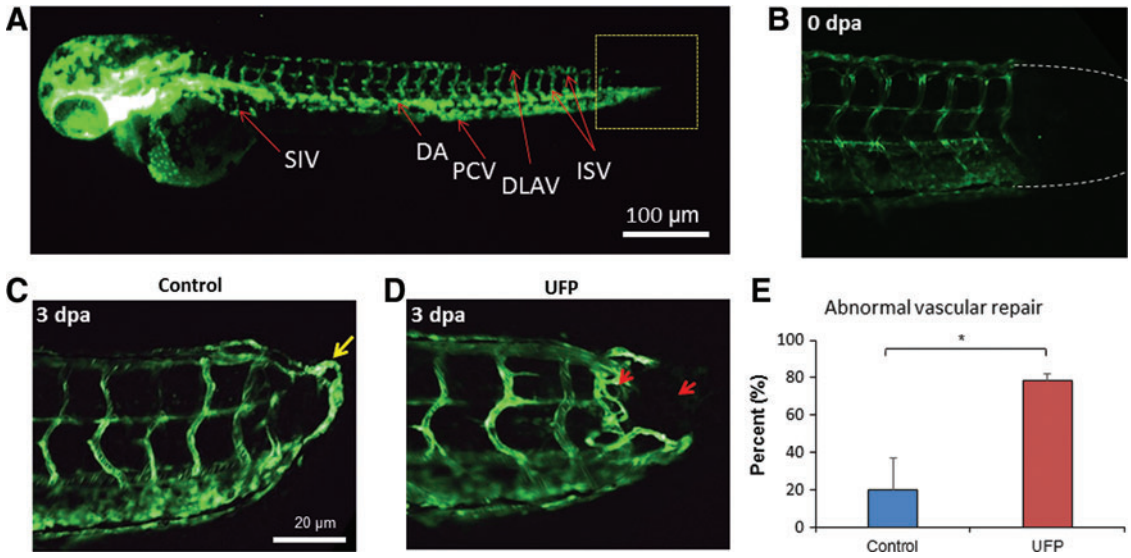

FIG. 1. UFP exposure impaired vascular regeneration. **(A)** Vasculature of transgenic *Tg(fli1:GFP)* zebrafish at 3 dpf. The *yellow dashed box* denotes the site of tail amputation. **(B)** Zebrafish underwent tail amputation at 3 dpf. *Dashed line* indicates the site of amputation. **(C)** Control fish developed vascular regeneration connecting the DA with the DLAV at 3 dpa (*yellow arrow*). **(D)** Fish exposed to UFP at 25 μg/mL developed impaired vascular repair and a disrupted vascular network (*red arrows*) at 3 dpa. **(E)** The proportion of fish with abnormal vascular repair. UFP exposure led to impaired vascular network formation (*$p < 0.05$, $n = 20$ for control, $n = 28$ for UFP). DA, dorsal aorta; DLAV, dorsal longitudinal anastomotic vessel; dpa, days post-amputation; dpf, days post-fertilization; UFP, ultrafine particles. To see this illustration in color, the reader is referred to the web version of this article at www.liebertpub.com/ars

Reduced endothelial Notch activity impaired vascular regeneration

We further crossbred the Notch reporter transgenic fish *Tg(tp1:GFP)* with *Tg(flk1:mCherry)* line to demonstrate Notch activity-mediated vascular regeneration. The *tp1* (Epstein Barr Virus terminal protein 1) in the Notch reporter line contains two Rbp-Jκ binding sites for NICD, thereby reporting regional Notch1b activation (28). Vascular endothelial Notch activity (as visualized in yellow) was reduced after UFP exposure, ADAM10 inhibitor treatment, or injection of DN-*Notch1b* mRNA, accompanied with incomplete vascular loop closure (*$p < 0.05$ *vs.* control, $n = 29$ for control, $n = 28$ for UFP, $n = 29$ for ADAM10, $n = 15$ for DN-*Notch1b*); whereas *NICD* mRNA injection rescued endothelial Notch activity and restored vascular regeneration (Fig. 4A). Endothelial Notch activity was further quantified by a customized MATLAB algorithm to color-code the accentuation of co-localized Notch activity in the vasculature (Fig. 4B). These findings further support that UFP exposure inhibits endothelial Notch activity to impair vascular network formation.

UFP exposure attenuated FOXO1-mediated Notch activation complex

To elucidate the mechanism underlying UFP-mediated reduction in Notch activity, we analyzed the protein levels of NICD and Notch co-activators to form the activation complex. The total, active, and nuclear NICD protein levels remained unchanged in HAEC after 6 h of UFP exposure (Fig. 5A). Consistently, intact level of NICD protein was observed in response to various UFP exposure time (2–6 h; *$p < 0.05$ *vs.* control, $n = 3$) (Supplementary Fig. S6). In contrast, FOXO1 expression, but not MAML1 expression, was significantly reduced after 6 h post-initial UFP exposure (*$p < 0.05$ *vs.* control, $n = 3$) (Fig. 5B). *FOXO1* mRNA expression was also reduced in a dose- and time-dependent manner by UFP treatment (*$p < 0.05$ *vs.* control, $n = 3$) (Fig. 5C). Treatment of the proteasome inhibitor, MG-132, in the presence of UFP restored UFP-attenuated FOXO1 protein expression, suggesting that UFP also stimulate the degradation of FOXO1 *via* proteasome (Fig. 5D) (*$p < 0.05$ *vs.* control, $n = 3$). To determine whether suppressing FOXO1 expression affects the formation of the Notch activation complex, we performed immunoprecipitation and immunofluorescence against NICD and FOXO1, respectively. Immunoprecipitation with different UFP exposure time (2–6 h) revealed that UFP suppressed FOXO1 expression 4–5 h post-initial exposure, whereas it significantly attenuated FOXO1-mediated NICD pull-down 5 and 6 h after exposure (Fig. 5E). Immunofluorescence further uncovered a reduction in NICD and FOXO1 co-localization (*$p < 0.05$, $n = 3$) (Fig. 5F). Silencing FOXO1 with small interfering RNA (siRNA) recapitulated the UFP-mediated reduction in Notch activation complex formation (*$p < 0.05$, $n = 3$) (Fig. 5E), and it down-regulated Notch signaling gene expression. These data corroborate FOXO1-mediated Notch signaling (Supplementary Fig. S7), and UFP suppression of FOXO1 expression, leading to a reduction in FOXO1/Notch activation complex.

FOXO1 is an essential co-activator for the Notch activation complex for vascular repair

To assess the importance of FOXO1/Notch activation complex for vascular regeneration, we performed gain- and loss-of-function analyses on FOXO1. Wholemount zebrafish

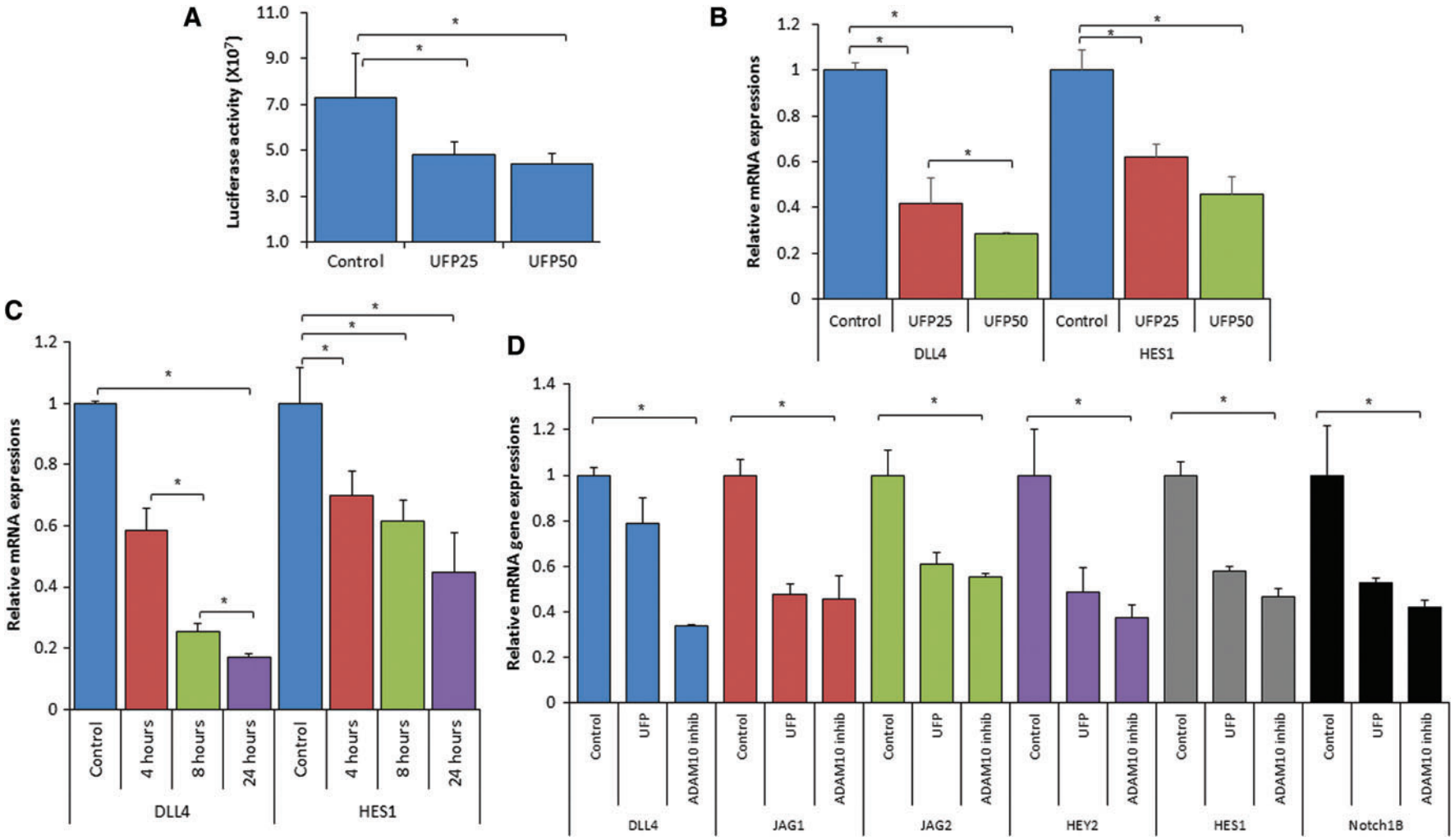

FIG. 2. UFP exposure down-regulated Notch-related genes. (A) HAEC transfected with Notch reporter plasmid pJH26 were treated with UFP at 25 μg/mL (UFP25) or 50 μg/mL (UFP50) for 12 h, resulting in a dose-dependent reduction in Luciferase activity (*$p < 0.05$ *vs.* control, $n = 3$). **(B)** Dose-dependent responses to UFP were compared in terms of mRNA expression of Notch ligand *Dll4* and Notch target *Hes1* in HAEC. **(C)** Time-dependent responses to UFP in the mRNA expression of *Dll4* and *Hes1*. UFP inhibited *Dll4* and *Hes1* in a dose- and time-dependent manner. **(D)** Notch signaling-related mRNA expression in zebrafish larvae, including Notch ligands, *Dll4* (*blue*), *JAG1* (*red*) and *JAG2* (*green*), Notch receptor, *Notch1b* (*black*), and Notch target gene *Hey2* (*purple*), was significantly down-regulated in response to UFP (25 μg/mL) or ADAM10 inhibitor (GI254023X at 5 μM) at 3 dpa (*$p < 0.05$ *vs.* control, $n = 3$). ADAM10, a disintegrin and metalloproteinase domain-containing protein 10; HAECs, human aortic endothelial cells; mRNA, messenger RNA. To see this illustration in color, the reader is referred to the web version of this article at www.liebertpub.com/ars

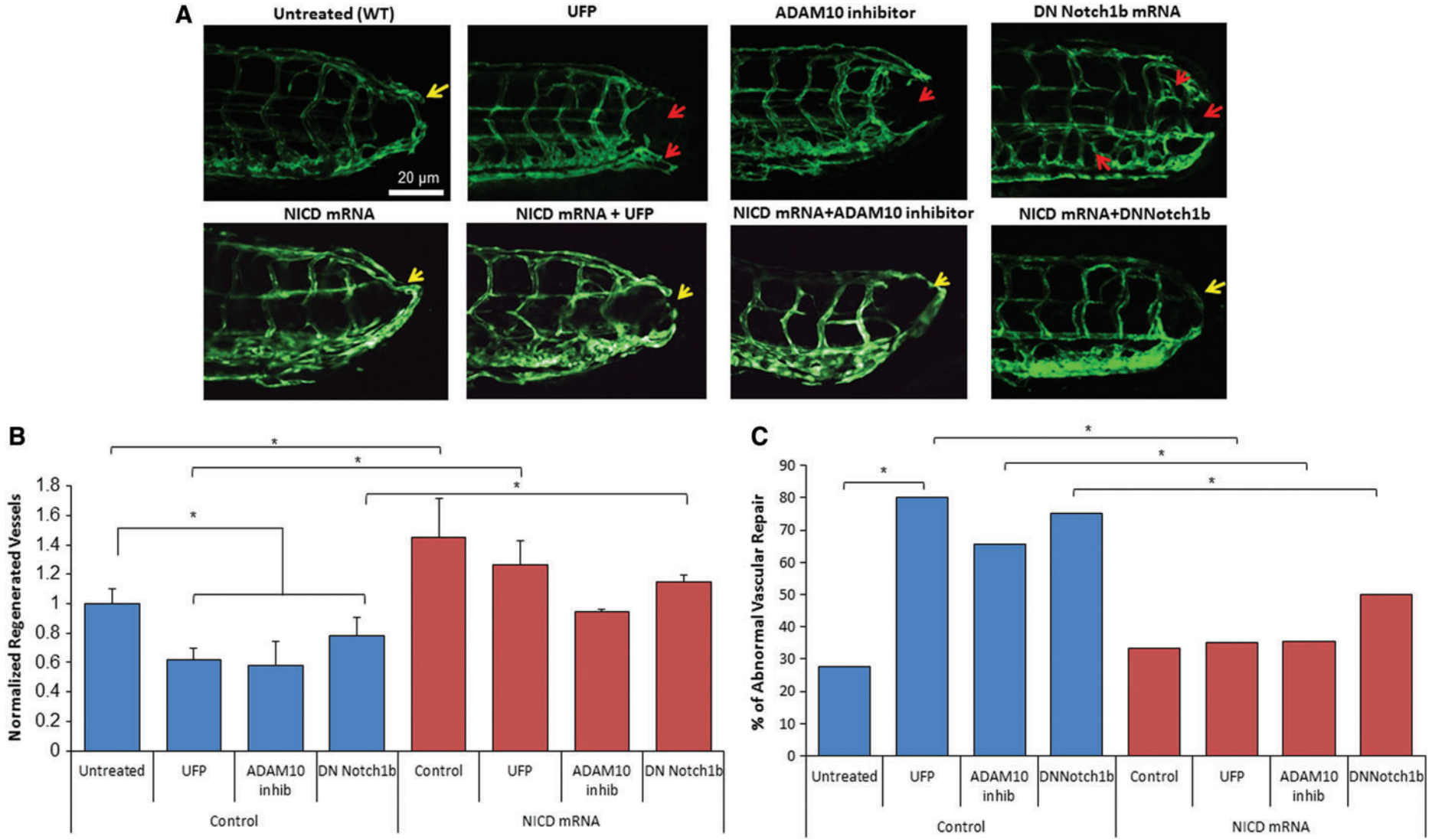

FIG. 3. UFP-attenuated Notch signaling impaired vascular regeneration. **(A)** Control *Tg(fli1: GFP)* zebrafish embryos developed vascular regeneration at 3 days post amputation (dpa). UFP or ADAM10 inhibitor treatment impaired vascular regeneration. Injection with DN-*Notch1b* mRNA mitigated ISV network and impaired tail regeneration (*$p < 0.05$, $n = 20$). *NICD* mRNA injection rescued UFP-, ADAM10 inhibitor-, or DN-*Notch1b* mRNA-impaired vascular regeneration. **(B)** Quantification of the area of regenerated vessels as described in the Materials and Methods section (*$p < 0.05$ *vs.* control, $n = 5$). **(C)** The proportion of fish with abnormal vascular regeneration was compared. DN, dominant negative; ISV, intersegmental vessel; NICD, notch intracellular cytoplasmic domain. To see this illustration in color, the reader is referred to the web version of this article at www.liebertpub.com/ars

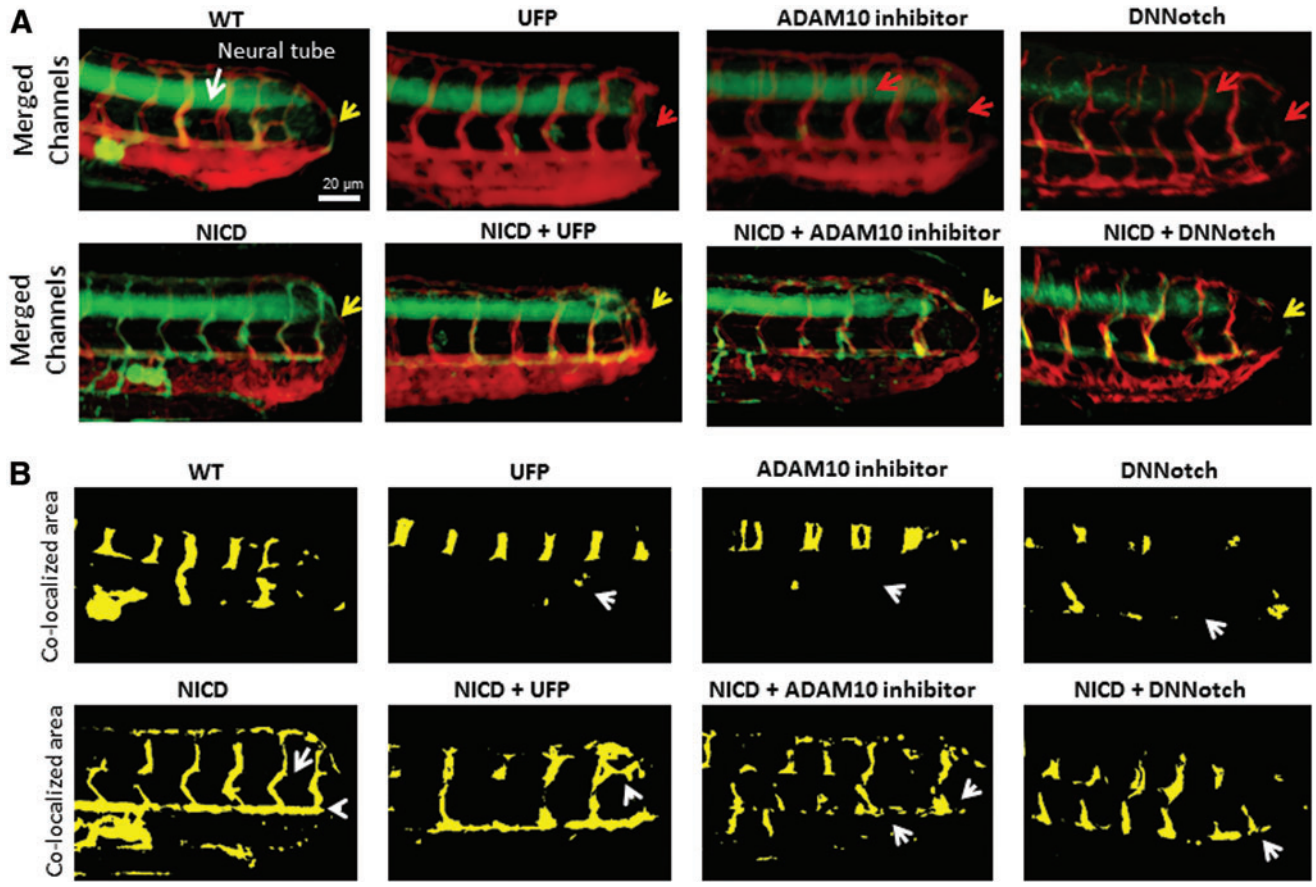

FIG. 4. Reduced endothelial Notch activity impaired vascular regeneration. (A) Transgenic *Tg(tp1:GFP; flk1:mCherry)* embryos revealed Notch activity in vasculature, as indicated by the overlapped *yellow color*, corroborating the role of endothelial Notch activity at the site of vascular repair (*yellow arrow*). **(B)** Endothelial Notch activity was quantified by customized MATLAB algorithm. In the presence of UFP, endothelial Notch activity was nearly absent, whereas *NICD* mRNA rescued UFP-, ADAM10 inhibitor, or DN-*Notch1b* mRNA-mediated reduction in Notch activity in the vasculature (*white arrows*). To see this illustration in color, the reader is referred to the web version of this article at www.liebertpub.com/ars

immunofluorescence staining with anti-FOXO1 validated the reduction of FOXO1 expression after FOXO1 morpholino oligonucleotide (MO) micro-injection (Supplementary Fig. S7A). Embryos injected with P53 control MO developed normal vascular repair at 3 dpa ($*p < 0.05$, $n = 20$), whereas FOXO1 MO impaired vascular regeneration analogous to UFP-mediated effect (Fig. 6A). *FOXO1* mRNA rescue restored regeneration despite the presence of UFP ($*p < 0.05$, $n = 25$), whereas co-injection of FOXO1 MO with *NICD* mRNA failed to restore vascular regeneration ($*p < 0.05$, $n = 17$) (Fig. 6A–C). FOXO1 MO attenuated Notch activity in the *Tg(tp1:GFP, flk1:mCherry)* embryos (Fig. 7 and Supplementary Fig. S7B), and co-injection of FOXO1 MO and *NICD* mRNA partially restored Notch activity ($*p < 0.05$, $n = 15$) (Fig. 7A, B). Taken together, FOXO1 is an essential co-activator of the Notch activation complex, and UFP inhibits FOXO1-mediated Notch signaling to impair vascular regeneration after tail amputation (Fig. 8).

FIG. 5. UFP exposure attenuated FOXO1-mediated Notch activation complex. (A) Total, active, and nuclear NICD protein expression remained unchanged after UFP exposure at 25 μg/mL for 6 h in HAEC. **(B)** Protein expressions of the NICD co-activator MAML1 was unchanged, whereas FOXO1 was significantly reduced after UFP exposure ($*p < 0.05$ *vs.* control, $n = 3$). **(C)** UFP down-regulated FOXO1 mRNA expression in a dose- and time-dependent manner ($*p < 0.05$ *vs.* control, $n = 3$). **(D)** HAEC were cultured in the presence or absence of UFP with or without 10 μM of proteasome inhibitor MG-132 for 6 h. FOXO1 protein expression were elevated by 1.34-fold when treated with MG-132 alone. UFP induced a decrease in FOXO1 protein expression, whereas MG-132 restored UFP-attenuated FOXO1 expression ($*p < 0.05$ *vs.* control, normalized to β-tubulin expression, $n = 3$). **(E)** Immunoprecipitation with different UFP exposure times (2–6 h) revealed significant reduction of FOXO1 and NICD pull-down against anti-FOXO1 antibody at 5 and 6 h post-UFP exposure, whereas the initial reduction started between 4 and 5 h of exposure ($*p < 0.05$ *vs.* control, $n = 3$). **(F)** Immunofluorescence staining of NICD and FOXO1 in HAEC treated with or without UFP. UFP significantly reduced FOXO1 levels (*white arrows*), whereas NICD levels remained unchanged. Co-localization with MATLAB code revealed that UFP reduced FOXO1-mediated Notch activation complex formation. FOXO1, forkhead box O-subfamily; MAML1, Master-mind like 1. To see this illustration in color, the reader is referred to the web version of this article at www.liebertpub.com/ars

Discussion

The novel contribution of our study lies in the elucidation of UFP-mediated disruption in FOXO1/Notch complex to impair vascular network formation. DN-*Notch 1b* mRNA injection or ADAM10 inhibitor treatment supports Notch signaling as the mechanism underlying UFP-impaired vascular regeneration. We further uncovered that UFP attenuated FOXO1 expression and FOXO1/NICD co-localization. Although *NICD* mRNA rescue partially restored Notch activity,

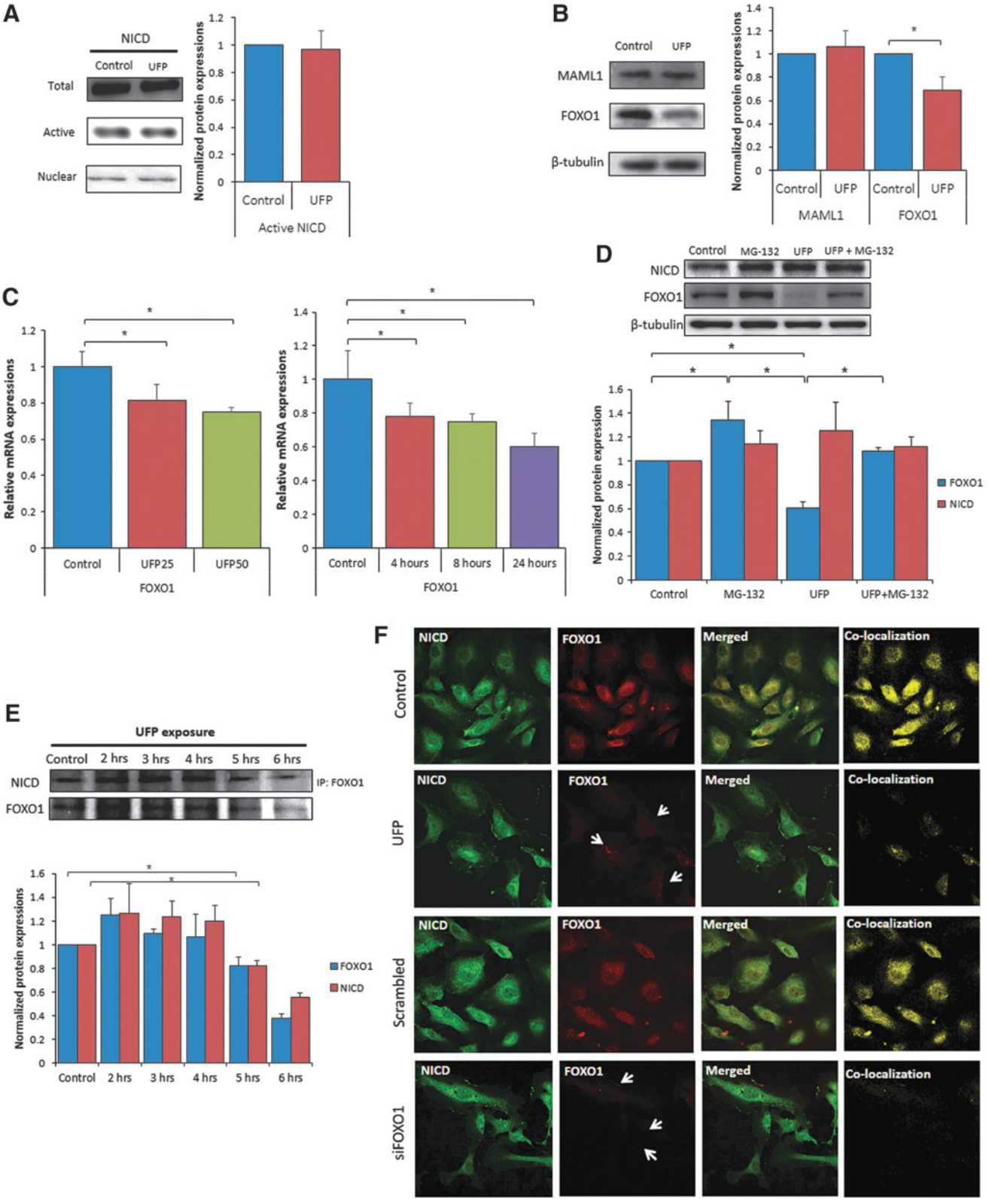

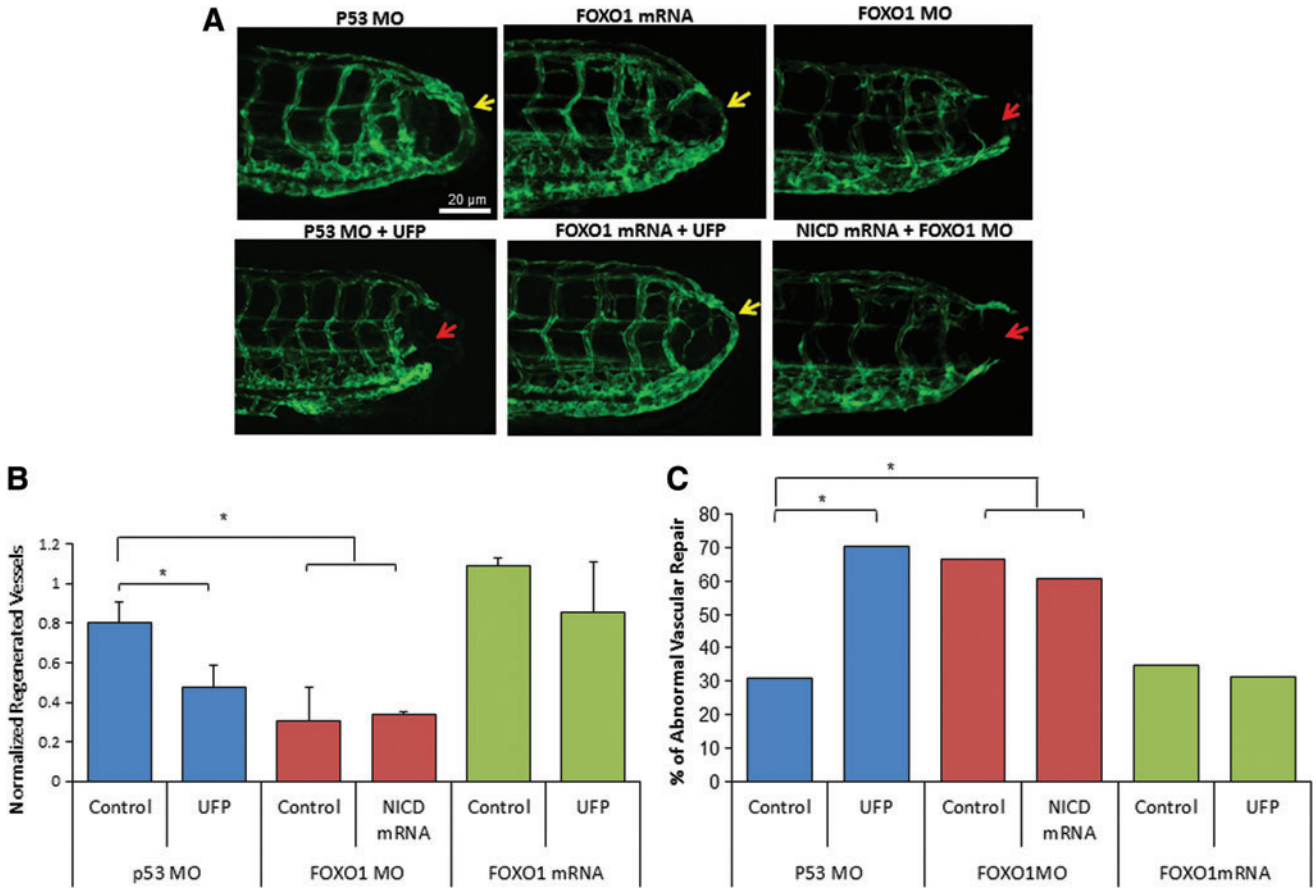

FIG. 6. UFP impairs vascular regeneration *via* FOXO1. **(A)** Transgenic *Tg(fli1:GFP)* zebrafish injected with P53 control MO developed vascular regeneration between the DA and DLAV (*yellow arrow*), but they impaired vascular regeneration in response to UFP treatment or FOXO1 MO injection (*red arrow*). Rescue with FOXO1 mRNA restored vascular regeneration in the presence of UFP (*yellow arrow*). Co-injection of NICD mRNA and FOXO1 MO failed to restore regeneration (*red arrow*). **(B)** The areas of regenerated vessels were quantified as described in the Materials and Methods section ($*p < 0.05$ *vs.* control, $n = 5$). **(C)** The proportion of fishes with abnormal vascular regeneration was quantified ($*p < 0.05$ *vs.* control, $n = 5$). MO, morpholino oligonucleotide. To see this illustration in color, the reader is referred to the web version of this article at www.liebertpub.com/ars

FOXO1 mRNA rescue completely restored UFP-attenuated Notch activity and blood flow to the injured site. Hence, FOXO1 is an essential co-activator for the Notch activation complex for Notch signaling-mediated vascular regeneration.

The Notch signaling pathway regulates stem cell differentiation and proliferation (6, 39, 51, 54, 61). Ablation of Notch1 induces developmental retardation, followed by collapsed arterial/venous specification and vascular malformation (27). Dysregulated Notch activity results in abnormal endothelial proliferation, leading to a hyperplastic vascular network that is prone to developing cancer (3). Missense mutation in the Notch3 gene is the underlying cause of the degenerative vascular disease known as Cerebral Autosomal-Dominant Arteriopathy with Subcortical Infarcts and Leukoencephalopathy (CADASIL) (23). In addition, Notch signaling is implicated in the initiation of sprouting angiogenesis (16, 37). After UFP exposure, zebrafish embryos developed impaired vascular repair and aberrant appearance in intersomatic space (Figs. 1 and 3), accompanied with reduced Notch activity and down-regulation of Notch target genes (Fig. 2). We further corroborated UFP-mediated reduction in Notch activity by using the transgenic *Tg(tp1:GFP)* Notch activity reporter line (Figs. 3 and 7). In addition, ADAM10 inhibitor or DN-*Notch1b* mRNA strengthened the role of Notch signaling in restoring vascular network formation. As a corollary, UFP attenuated vascular endothelial cell migration and tube formation (Supplementary Fig. S2). Thus, UFP attenuates Notch signaling to impair vascular regeneration.

NICD, MAML1, and FOXO1 bind to the CSL domain to form a Notch activation complex. Although UFP inhibited Notch activity, NICD and MAML protein levels remained unchanged. For this reason, we uncovered down-regulation of FOXO1 mRNA and protein expression after UFP exposure (Fig. 5). FOXO1 and Notch cooperation has been reported in myogenic differentiation and neural stem cell differentiation (25, 26). Our data suggest that UFP exposure suppressed FOXO1-mediated Notch activation complex formation, thus attenuating Notch signaling for vascular regeneration.

Exposure to ambient $PM_{2.5}$ promotes cardiovascular, pulmonary, and gastrointestinal disorders (7). Epidemiological studies associated maternal exposure to air pollutants with increased occurrence of congenital heart diseases (12). Maternal exposure to ozone (O_3) at the second-month gestation increases the risk of aortic and pulmonary valve

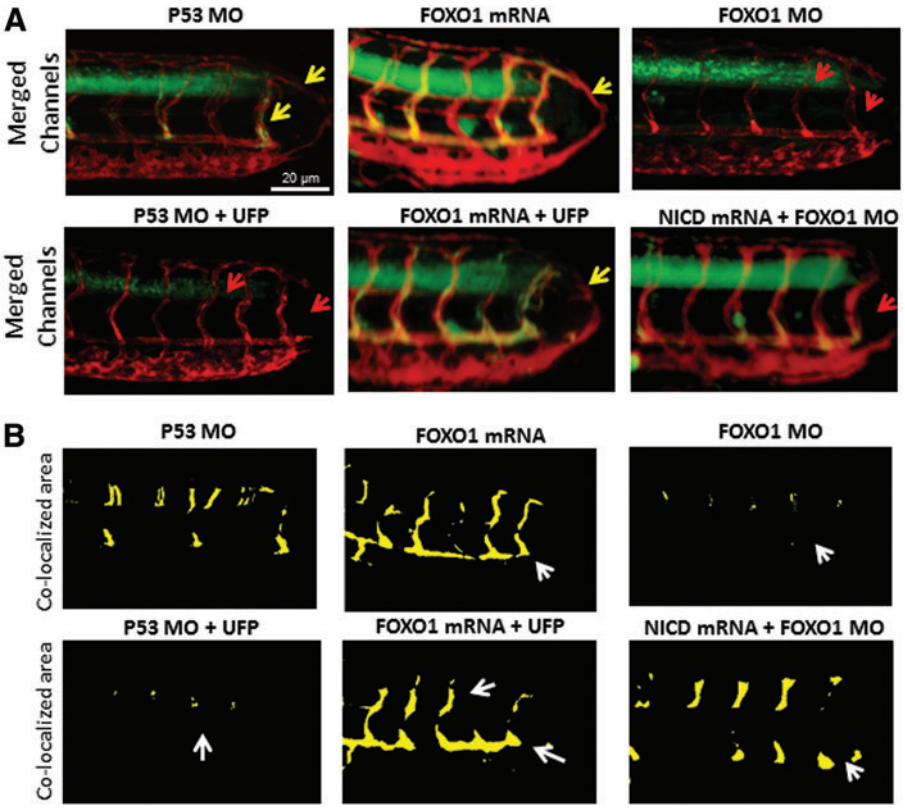

FIG. 7. FOXO1 modulated endothelial Notch activity at the site of vascular injury. (A) In the transgenic *Tg(tp1:GFP; flk1:mCherry)* embryos, FOXO1 MO attenuated Notch activity and impaired vascular regeneration (*red arrows*). Rescue with FOXO1 mRNA promoted endothelial Notch activity and reversed UFP-impaired vascular regeneration ($*p < 0.05$ *vs.* control, $n = 26$) (*yellow arrow*). Co-injection of *NICD* mRNA with FOXO1 MO partially restored Notch activity, but it failed to restore vascular regeneration (*red arrow*). **(B)** Endothelial Notch activity was quantified by the customized MATLAB code. Endothelial Notch activity was attenuated (*white arrows*) in response to UFP exposure or to FOXO1 MO, whereas rescue with *FOXO1* mRNA restored Notch activity. To see this illustration in color, the reader is referred to the web version of this article at www.liebertpub.com/ars

anomalies (52). UFP are the redox-active sub-fraction of $PM_{2.5}$, harboring elemental carbon and polycyclic aromatic hydrocarbons as products of incomplete combustion from urban environmental sources, including the exhaust from diesel trucks and gasoline vehicles (30). Their large surface-to-volume ratio favors their potential adsorption to or absorption in the pulmonary and cardiovascular systems (13, 44, 56). Long-term epidemiological studies on UFP exposure demonstrate adverse respiratory function (40, 49), exercise-induced cardiac ischemia (47), and arrhythmias (17). At the molecular level, UFP induces JNK-mediated superoxide ($O_2^{\cdot -}$) production and NF-κB-mediated monocyte recruitment to prime atherosclerosis (32, 34). UFP exposure *via* inhalation increases plasma lipid metabolites and reduces high density lipoprotein (HDL) anti-oxidant capacity to accelerate atherosclerosis in low density lipoprotein receptor (LDLR)-null mice (31). UFP inhalation further promotes atherogenic lipid metabolites and macrophage infiltrates in

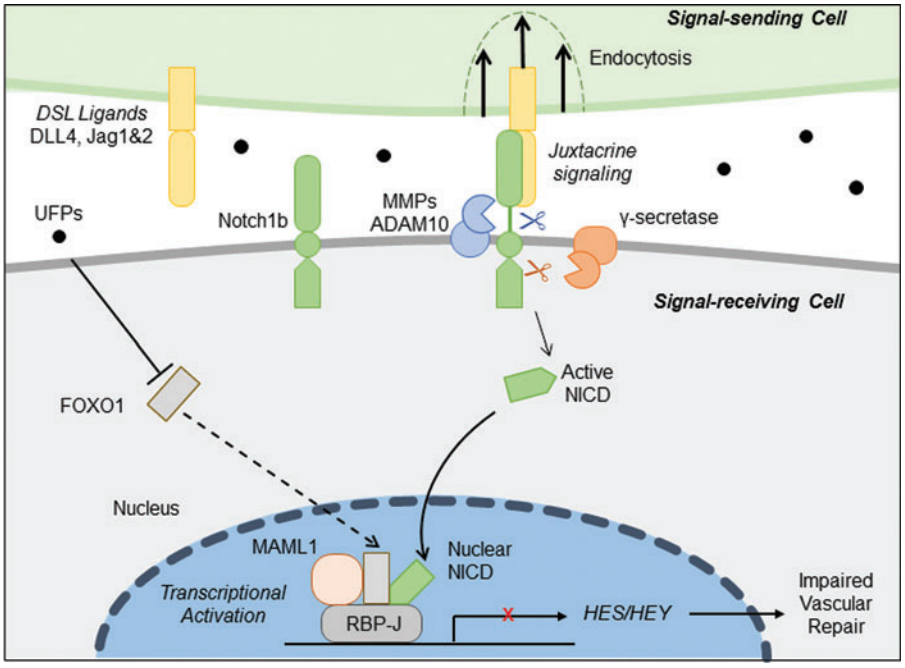

FIG. 8. A schematic diagram. A depiction of the disruption of FOXO1/Notch cooperation highlights impaired vascular network formation. To see this illustration in color, the reader is referred to the web version of this article at www.liebertpub.com/ars

the intestine (30), where microbiota composition was altered to produce atherogenic lipid metabolites (35). In our zebrafish model of vascular injury and repair, we provide the first molecular insights into UFP-suppressed FOXO1 as a co-activator for the Notch activation complex.

The emerging role of redox-sensitive microRNAs (miRNAs), including miR-223 and –375, has been implicated in disrupting FOXO1 signaling (45) and cellular proliferation (63, 65). Further, miR-154 and –379 have been reported to regulate inflammatory responses (21, 46). Although miR-3188 targets the mTOR pathway to suppress p-PI3K/p-AKT/c-JUN signaling (67), miR-132 activates the PI3K/AKT pathway to decrease FOXO1 expression (36). $PM_{2.5}$ has been reported to modulate the levels of a number of miRNAs, including miR-223 and miR-375 (5, 53, 64). Thus, UFP could down-regulate FOXO1 by modulating miRNAs. In addition, we have previously reported that UFP activates JNK, and JNK activation promotes protein ubiquitination and degradation *via* proteasome activity (32, 59). In this study, we observed that UFP down-regulated FOXO1 protein levels *via* proteasome degradation (Fig. 5D), which could be mediated by the JNK pathway (Supplementary Fig. S9). However, the precise mechanism whereby UFP exposure suppresses FOXO1 expression warrants further investigation (19).

Overall, we demonstrate FOXO1 as an important co-activator with NICD for assembling the Notch activation complex for vascular development and regeneration (11). UFP-mediated reduction in FOXO1/NICD complex formation was corroborated by immunoprecipitation of FOXO1-mediated NICD pull-down, immunofluorescence of FOXO1 expression, and FOXO1/NICD co-localization. Thus, exposure to redox-active UFP disrupts Notch activity to impair vascular network formation.

Materials and Methods

UFP collection

UFP were collected at the University of Southern California (USC) campus near downtown Los Angeles, California. UFP are characterized by a mixture of particulate pollutants, including ambient PM from heavy duty diesel trucks, light duty gasoline vehicles, and PM generated by photochemical oxidation of primary organic vapors (60). UFP were collected with High-Volume Particle Sampler, operating at 400 L/min (42), on Zefluor PTFE membrane filters (3 μm; Pall Life Sciences). Collected PM samples were extracted from the filter substrates by soaking and vortexing in ultrapure Milli-Q water followed by sonication and neutralization. Metal and organic content of the UFP samples was quantified by using inductively coupled plasma mass spectrometry and Siever 900 Organic Carbon Analyzer, respectively, as reported (18, 58). Mass fraction of the total organic carbon and major metals (in units of ng/μg UFP) are summarized in Supplementary Figure S1.

Vascular endothelial cell culture and exposure to UFP

HAECs were cultured in endothelial growth medium (Cell Applications, San Diego, CA) supplemented with 5% fetal bovine serum (FBS), 1% penicillin/streptomycin (Life Technologies), and 0.1% fungicide. HAEC were propagated for experiments between passages 4 and 7, and were treated with UFP, ADAM10 inhibitor, GI254023X, or proteasome inhibitor, MG-132 (Sigma-Aldrich, St. Louis, MO) at indicated concentrations diluted in M199 media (Life Technologies).

*Preparation of NICD, FOXO1, and DN-*Notch1b *mRNA*

Rat NICD and mouse FOXO1 complementary DNA (cDNA) were amplified from donor plasmids and cloned into the plasmid pCS2+ at the *Bam*HI/*Eco*RI sites (for NICD) and *Bam*HI/*Xba*I sites (for FOXO1), respectively. Zebrafish DN-*Notch1b* cDNA was amplified from zebrafish cDNA with primers excluding the intracellular domain and cloned into pCS2+ at *Eco*RI/*Xho*I sites. Clones with insert of interest were selected by polymerase chain reaction (PCR) screening and validated with sequencing. mRNAs were prepared by using the mMessage SP6 kit (Invitrogen) by following the manufacturer's instruction. The *in vitro* transcribed mRNAs were purified by using a total RNA isolation kit (Bio-Rad) for *in vivo* rescue experiments.

Notch reporter activity assay

HEK-293 cells were grown to sub-confluence in 24-well plates. The cells were transfected with the Notch reporter plasmid pJH26 with or without control or DN-*Notch1b* plasmid overnight by using Lipofectamine 2000 (Thermo Fisher Scientific). The cells were treated overnight with UFP at different concentrations in M199 containing 0.1% FBS. The cells were lysed in Passive Lysis Buffer (Promega), and luciferase activities were quantified with a Luminometer using Bright-Glow substrate (Promega).

Quantitative real-time PCR analysis

Notch signaling-related gene mRNA expression patterns, including Notch ligands *DLL4, JAG1* and *JAG2*, Notch receptor *Notch1b*, downstream target *Hey2*, and *FOXO1*, were assessed by quantitative real-time PCR. RNA was isolated by using the Bio-Rad total RNA kit (Bio-Rad), and it was synthesized into cDNA by using the iScript cDNA synthesis kit (Bio-Rad). Synthesized cDNAs were diluted in the molecular biology reagent water (Sigma-Aldrich) for PCR amplification with qPCR master mix (Applied Biological Materials, Inc.). The individual mRNA expression patterns were normalized to actin expression. Sequences of primers and MOs are listed in Table 1.

Western blot analysis and immunoprecipitation

HAEC treated with or without UFP were lysed with standard RIPA buffer supplemented with phosphatase inhibitor as previously described (33). Cytosolic and nuclear lysates were prepared as previously described (29). Protein concentrations of each sample were determined by DCP assay. Western blotting was done as previously described (33) with anti-FOXO1 (H-128; Santa Cruz Biotechnology, Inc.), anti-MAML1 (EMD Millipore, Inc.), and anti-NICD (V1744; Cell Signaling Technology, Inc.). Equal loading was verified with anti-β-tubulin (AA2; Santa Cruz Biotechnology, Inc.). Blot densitometry was performed with the FluorChem FC2 imaging software for chemiluminescence. Immunoprecipitation of FOXO1 and NICD was performed with Pierce Crosslink magnetic IP/CI-IP kit (Thermo Fisher Scientific) by following the manufacturer's instruction. Elution of

Table 1. Sequencing Information of Quantitative Real-Time Polymerase Chain Reaction Primers and Morpholino

Human		
Hey1	Forward	GTTCGGCTCTAGGTTCCATGT
	Backward	CGTCGGCGCTTCTCAATTATTC
Dll4	Forward	CGACAGGTGCAGGTGTAGC
	Backward	TACTTGTGATGAGGGCTGGG
FOXO1	Forward	GCGACCTGTCCTACGCCGACCTCA
	Backward	CCTTGAAGTAGGGCACGCTCTTGACC
Zebrafish		
Jag1	Forward	CCGCGTATGTTTGAAGGAGTATCAGTCG
	Backward	CAGCACGATCCGGGTTTTGTCG
Jag2	Forward	AGCCCTAGCAAAACGAGCGACG
	Backward	GCGTGAATGTGCCGTTCGATCAA
Dll4	Forward	CAAAGTGGGAAGCAGACAGAGCTAAGG
	Backward	CGGTCATCCCTGGGTGTGCATT
Notch1b	Forward	CAGAGAGTGGAGGCACAGTGCAATCC
	Backward	GCCGTCCCATTCACACTCTGCATT
Hey2	Forward	AAGATGTGGCTCACCTACAAC
	Backward	TGGCACCAGACGACGCAACTC
FOXO1	Forward	TTGTTCTTTTTGCAGGATCCACCATGGCCGAGGCGCCCCAGGTG
	Backward	TCACTATAGTTCTAGATTAGCCTGACACCCAGCTGTGTGTTGTAG
NICD	Forward	GCAGGATCCACCATGGGTTGTGGGGTGCTGCTGTCCCGCAAG
	Backward	CTTGAATTCTTACTTAAATGCCTCTGGAATGTGGGTG
DN-Notch1b	Forward	GATCCCATCGATTCGAATTCACCATGCATCTTTTCTTCGTGA AACTAATTGTTG
	Backward	CTATAGTTCTAGAGGCTCGAGCTAAGCGTAATCTGGAA CATCGTATGGGTATTCTCCGACCGGCTCTCTCCTC
P53 MO		GCGCCATTGCTTTGCAAGAATTG
FOXO1 MO		CTTTGAGGGCCATTACCTTCCAGCC

DN, dominant negative; FOXO1, forkhead box O-subfamily; MO, morpholino oligonucleotide; NICD, notch intracellular cytoplasmic domain.

imunoprecipitation was neutralized with neutralize buffer (Thermo Fisher Scientific) for Western blot analysis.

Assessment of vascular regeneration with the transgenic Tg(fli1:GFP) *zebrafish tail amputation model*

The transgenic *Tg(fli1:GFP)* zebrafish line, in which vascular endothelial cells were labeled with GFP under the promoter of *Fli1* (also known as *ERGB*), was used to image the vascular regeneration. *Tg(fli1:GFP)* fish embryos were injected with or without NICD mRNA, P53 control MO (GeneTools, LLC), FOXO1 MO (GeneTools, LLC), FOXO1 mRNA (2–4 pg), or *DN-Notch1b* mRNA, and they were cultured in standard E3 medium supplemented with 0.05% methylene blue at 28.5°C for 3 days. At 3 dpf, $\sim 100\,\mu$m of the posterior tail segments was amputated by using a clean razor blade under a phase-contrast microscope (Zeiss). Embryos were then returned to fresh E3 medium, or E3 medium with UFP or ADAM10 inhibitor. At 3 dpa, embryonic zebrafish were randomly picked and immobilized in neutralized 0.02% tricaine solution (Sigma-Aldrich), and they were mounted in 1–2% low-melting agarose (Sigma-Aldrich) on a glass coverslip to image regeneration of blood vessels with confocal microscopy (Zeiss).

Notch activity in double transgenic Tg(tp1:GFP; flk1:mCherry) *embryos*

The *Tg(tp1:GFP)* Notch reporter line was crossbred with the *Tg(flk1:mCherry)* line to localize endothelial Notch signaling. NICD mRNA, FOXO1 MO, and FOXO1 mRNA were micro-injected to modulate Notch signaling and to elucidate FOXO1/Notch cooperation. At 6 dpf (3 dpa), embryos were randomly selected to image Notch activation in the central nervous system and in the amputated tail. Embryos from the remaining group were sorted and treated with and without UFP and ADAM10 inhibitor. After 3 days of treatment, Notch signaling localized in the vasculature was scanned at 3–5 μm intervals in the Z direction by using dual-channel confocal microscopy (Zeiss). Images of Notch activity and the vascular endothelial layer were acquired and superimposed to visualize endothelial Notch activation. Images from each channel are displayed as Supplementary Figure S8. Stacked images from both channels were projected onto a single plane by using ImageJ to visualize three-dimensional (3D) Notch activation.

Immunofluorescence staining

After UFP exposure, HAECs were fixed with 4% paraformaldehyde (PFA) and stained with antibody against NICD and FOXO1 diluted in 2% bovine serum albumin (BSA; Sigma-Aldrich). Images were acquired by using dual-channel confocal microscopy (Zeiss) and superimposed by using ImageJ.

Visualization of FOXO1/NICD co-localization

To accentuate co-localization of NICD and FOXO1, we customized a MATLAB (Mathworks) algorithm. Multi-level image thresholds were applied for segmenting the single slice

in each channel. Threshold levels for each channel were manually chosen to generate binary masks of the slice. Pixels defined with binary masks were merged together and visualized as overlapping regions, whereas the remaining regions were regarded as background.

FOXO1 knockdown

Scrambled (Qiagen) and FOXO1 siRNA (Thermo Fisher Scientific) were transfected to HAEC with Lipofectamine 2000 (Invitrogen) as previously described (32). To confirm FOXO1 knockdown, cells were applied to immunofluorescence staining and imaged under fluorescent microscopy (Zeiss) at 48 h post-transfection.

Endothelial cell migration and tube formation assays

For migration assays, HAEC monolayers at confluence were scratched with 200 μL pipette tips. After the scratch, cells were treated with or without UFP at 25 μg/mL in M199 media (Life Technologies). Cell migration was imaged under phase-contrast microscopy (Olympus IX 70) at 4, 8, 12, and 24 h. For the quantification of cell migration, distances between each inner border of cells were assessed by using ImageJ. For tube formation assays, confluent HAEC were pre-treated with or without UFP at 25 μg/mL and re-suspended in Dulbecco's modified Eagle's medium (Invitrogen) supplemented with 25 ng/mL VEGF and 5% FBS. Cells were then added to 96-well plates coated with growth factor-reduced Matrigel (BD Biosciences) and were incubated with or without UFP. Tube formation was imaged under phase-contrast microscopy at 4, 8, 12, and 24 h.

Quantification of the regenerated intersegmental vessels

To quantify changes in vascular repair, we used Amira 3D imaging software. The whole vasculature on the posterior tail segment was masked (purple). The area of regenerated vessels was derived manually by designating segmental vessels (pink) connecting the DA and the DLAV (Supplementary Fig. S4).

Imaging blood flow on the tail post-regeneration

Double transgenic *Tg(fli1:GFP; gata1:DS-RED)* zebrafish underwent tail amputation at 3 dpf, and they were maintained with or without UFP at 25 μg/mL for 3 days. At 3 dpa, fish were immobilized and placed in 1–2% low-melting agarose to image the circulation of erythrocytes through the regenerated vessel. Images of the blood flow and endothelial layer were taken separately with QIcam at 20–30 frames per second. Images were superimposed by using Corel imaging software.

Wholemount zebrafish immunofluorescence staining

WT zebrafish embryos were injected with P53 MO and FOXO1 MO (GeneTools, LLC), respectively, and they were maintained in standard E3 medium at 28.5°C for 3 days. At 3 dpf, embryos were fixed in 4% PFA solution overnight and were subjected to pure acetone for dehydration. Embryos were then rehydrated with 0.2% PBST and were blocked with 2% BSA (Sigma-Aldrich). Zebrafish embryos underwent 24 h of incubation with FOXO1-targeted antibody (C-9; Santa Cruz Biotechnology, Inc.) to assess reduction of FOXO1. Fluorescent images were acquired by using a confocal microscope (Zeiss) by mounting embryos in 1–2% low-melting agarose.

Statistical analysis

Data were expressed as mean ± standard deviation and compared among separate experiments. Unpaired two-tail *t* test and two-proportion *z*-test were used for statistical comparisons between two experimental conditions. *p* Values <0.05 were considered significant. Comparisons of multiple values were made by one-way analysis of variance, and statistical significance for pairwise comparison was determined by using the Tukey test.

Acknowledgments

The authors are grateful to Dr. Weinmaster for providing the NICD plasmid and the JH26 Notch reporter plasmid, and they thank Drs. David Traver at UCSD and Nathan Lawson at the University of Massachusetts Medical School (Worcester, MA) for generously providing the *Tg(tp1:GFP)* line. This study was supported by National Institutes of Health R01HL083015 (T.K.H.), R01HL111437 (T.K.H.), R01HL129727 (T.K.H.), R01HL118650 (T.K.H.), and the American Heart Association 16SDG30910007 (R.R.S.P.), and it was funded by EPA under STAR program (C.S.) and the South Coast Air Quality Management District Award (C.S.).

Author Disclosure Statement

No competing financial interests exist.

References

1. Accili D and Arden KC. FoxOs at the crossroads of cellular metabolism, differentiation, and transformation. *Cell* 117: 421–426, 2004.
2. Araujo JA, Barajas B, Kleinman M, Wang X, Bennett BJ, Gong KW, Navab M, Harkema J, Sioutas C, Lusis AJ, and Nel AE. Ambient particulate pollutants in the ultrafine range promote early atherosclerosis and systemic oxidative stress. *Circ Res* 102: 589–596, 2008.
3. Artavanis-Tsakonas S, Rand MD, and Lake RJ. Notch signaling: cell fate control and signal integration in development. *Science* 284: 770–776, 1999.
4. Baonza A and Garcia-Bellido A. Notch signaling directly controls cell proliferation in the Drosophila wing disc. *Proc Natl Acad Sci U S A* 97: 2609–2614, 2000.
5. Bleck B, Grunig G, Chiu A, Liu M, Gordon T, Kazeros A, and Reibman J. MicroRNA-375 regulation of thymic stromal lymphopoietin by diesel exhaust particles and ambient particulate matter in human bronchial epithelial cells. *J Immunol* 190: 3757–3763, 2013.
6. Bray SJ. Notch signalling in context. *Nat Rev Mol Cell Biol* 17: 722–735, 2016.
7. Brook RD, Franklin B, Cascio W, Hong Y, Howard G, Lipsett M, Luepker R, Mittleman M, Samet J, Smith SC, Jr, and Tager I; Expert Panel on Population and Prevention Science of the American Heart Association. Air pollution and cardiovascular disease: a statement for healthcare professionals from the Expert Panel on Population and Prevention Science of the American Heart Association. *Circulation* 109: 2655–2671, 2004.

8. Brook RD and Rajagopalan S. Particulate matter air pollution and atherosclerosis. *Curr Atheroscler Rep* 12: 291–300, 2010.
9. Brook RD, Rajagopalan S, Pope CA, 3rd, Brook JR, Bhatnagar A, Diez-Roux AV, Holguin F, Hong Y, Luepker RV, Mittleman MA, Peters A, Siscovick D, Smith SC, Jr, Whitsel L, and Kaufman JD; American Heart Association Council on Epidemiology and Prevention, Council on the Kidney in Cardiovascular Disease, and Council on Nutrition, Physical Activity and Metabolism. Particulate matter air pollution and cardiovascular disease: an update to the scientific statement from the American Heart Association. *Circulation* 121: 2331–2378, 2010.
10. Brunekreef B and Holgate ST. Air pollution and health. *Lancet* 360: 1233–1242, 2002.
11. Chavez MN, Aedo G, Fierro FA, Allende ML, and Egana JT. Zebrafish as an emerging model organism to study angiogenesis in development and regeneration. *Front Physiol* 7: 56, 2016.
12. Dadvand P, Rankin J, Rushton S, and Pless-Mulloli T. Ambient air pollution and congenital heart disease: a register-based study. *Environ Res* 111: 435–441, 2011.
13. Frampton MW. Systemic and cardiovascular effects of airway injury and inflammation: ultrafine particle exposure in humans. *Environ Health Perspect* 109: 529–532, 2001.
14. Fre S, Huyghe M, Mourikis P, Robine S, Louvard D, and Artavanis-Tsakonas S. Notch signals control the fate of immature progenitor cells in the intestine. *Nature* 435: 964–968, 2005.
15. Gorham ED, Garland CF, and Garland FC. Acid haze air pollution and breast and colon cancer mortality in 20 Canadian cities. *Can J Public Health* 80: 96–100, 1989.
16. Hellstrom M, Phng LK, Hofmann JJ, Wallgard E, Coultas L, Lindblom P, Alva J, Nilsson AK, Karlsson L, Gaiano N, Yoon K, Rossant J, Iruela-Arispe ML, Kalen M, Gerhardt H, and Betsholtz C. Dll4 signalling through Notch1 regulates formation of tip cells during angiogenesis. *Nature* 445: 776–780, 2007.
17. Henneberger A, Zareba W, Ibald-Mulli A, Ruckerl R, Cyrys J, Couderc JP, Mykins B, Woelke G, Wichmann HE, and Peters A. Repolarization changes induced by air pollution in ischemic heart disease patients. *Environ Health Perspect* 113: 440–446, 2005.
18. Herner JD, Green PG, and Kleeman MJ. Measuring the trace elemental composition of size-resolved airborne particles. *Environ Sci Technol* 40: 1925–1933, 2006.
19. Huang T, Wang-Johanning F, Zhou F, Kallon H, and Wei Y. MicroRNAs serve as a bridge between oxidative stress and gastric cancer (review). *Int J Oncol* 49: 1791–1800, 2016.
20. Hwang BF, Lee YL, and Jaakkola JJ. Air pollution and the risk of cardiac defects: a population-based case-control study. *Medicine (Baltimore)* 94: e1883, 2015.
21. Izzotti A, Larghero P, Balansky R, Pfeffer U, Steele VE, and De Flora S. Interplay between histopathological alterations, cigarette smoke and chemopreventive agents in defining microRNA profiles in mouse lung. *Mutat Res* 717: 17–24, 2011.
22. Jensen J, Heller RS, Funder-Nielsen T, Pedersen EE, Lindsell C, Weinmaster G, Madsen OD, and Serup P. Independent development of pancreatic alpha- and beta-cells from neurogenin3-expressing precursors: a role for the notch pathway in repression of premature differentiation. *Diabetes* 49: 163–176, 2000.
23. Joutel A, Corpechot C, Ducros A, Vahedi K, Chabriat H, Mouton P, Alamowitch S, Domenga V, Cecillion M, Marechal E, Maciazek J, Vayssiere C, Cruaud C, Cabanis EA, Ruchoux MM, Weissenbach J, Bach JF, Bousser MG, Tournier-and Lasserve E. Notch3 mutations in CADASIL, a hereditary adult-onset condition causing stroke and dementia. *Nature* 383: 707–710, 1996.
24. Karimi Galougahi K, Ashley EA, and Ali ZA. Redox regulation of vascular remodeling. *Cell Mol Life Sci* 73: 349–363, 2016.
25. Kim DY, Hwang I, Muller FL, and Paik JH. Functional regulation of FoxO1 in neural stem cell differentiation. *Cell Death Differ* 22: 2034–2045, 2015.
26. Kitamura T, Kitamura YI, Funahashi Y, Shawber CJ, Castrillon DH, Kollipara R, DePinho RA, Kitajewski J, and Accili D. A Foxo/Notch pathway controls myogenic differentiation and fiber type specification. *J Clin Invest* 117: 2477–2485, 2007.
27. Krebs LT, Xue Y, Norton CR, Shutter JR, Maguire M, Sundberg JP, Gallahan D, Closson V, Kitajewski J, Callahan R, Smith GH, Stark KL, and Gridley T. Notch signaling is essential for vascular morphogenesis in mice. *Genes Dev* 14: 1343–1352, 2000.
28. Lee J, Fei P, Packard RR, Kang H, Xu H, Baek KI, Jen N, Chen J, Yen H, Kuo CC, Chi NC, Ho CM, Li R, and Hsiai TK. 4-Dimensional light-sheet microscopy to elucidate shear stress modulation of cardiac trabeculation. *J Clin Invest* 126: 1679–1690, 2016.
29. Li R, Chen W, Yanes R, Lee S, and Berliner JA. OKL38 is an oxidative stress response gene stimulated by oxidized phospholipids. *J Lipid Res* 48: 709–715, 2007.
30. Li R, Navab K, Hough G, Daher N, Zhang M, Mittelstein D, Lee K, Pakbin P, Saffari A, Bhetraratana M, Sulaiman D, Beebe T, Wu L, Jen N, Wine E, Tseng CH, Araujo JA, Fogelman A, Sioutas C, Navab M, and Hsiai TK. Effect of exposure to atmospheric ultrafine particles on production of free fatty acids and lipid metabolites in the mouse small intestine. *Environ Health Perspect* 123: 34–41, 2015.
31. Li R, Navab M, Pakbin P, Ning Z, Navab K, Hough G, Morgan TE, Finch CE, Araujo JA, Fogelman AM, Sioutas C, and Hsiai T. Ambient ultrafine particles alter lipid metabolism and HDL anti-oxidant capacity in LDLR-null mice. *J Lipid Res* 54: 1608–1615, 2013.
32. Li R, Ning Z, Cui J, Khalsa B, Ai L, Takabe W, Beebe T, Majumdar R, Sioutas C, and Hsiai T. Ultrafine particles from diesel engines induce vascular oxidative stress via JNK activation. *Free Radic Biol Med* 46: 775–782, 2009.
33. Li R, Ning Z, Cui J, Yu F, Sioutas C, and Hsiai T. Diesel exhaust particles modulate vascular endothelial cell permeability: implication of ZO-1 expression. *Toxicol Lett* 197: 163–168, 2010.
34. Li R, Ning Z, Majumdar R, Cui J, Takabe W, Jen N, Sioutas C, and Hsiai T. Ultrafine particles from diesel vehicle emissions at different driving cycles induce differential vascular pro-inflammatory responses: implication of chemical components and NF-kappaB signaling. *Part Fibre Toxicol* 7: 6, 2010.
35. Li R, Yang J, Saffari A, Jacobs J, Baek KI, Hough G, Larauche MH, Ma J, Jen N, Moussaoui N, Zhou B, Kang H, Reddy S, Henning SM, Campen MJ, Pisegna J, Li Z, Fogelman AM, Sioutas C, Navab M, and Hsiai TK. Ambient ultrafine particle ingestion alters gut microbiota in associ-

ation with increased atherogenic lipid metabolites. *Sci Rep* 7: 42906, 2017.
36. Lian R, Lu B, Jiao L, Li S, Wang H, Miao W, and Yu W. MiR-132 plays an oncogenic role in laryngeal squamous cell carcinoma by targeting FOXO1 and activating the PI3K/AKT pathway. *Eur J Pharmacol* 792: 1–6, 2016.
37. Lobov IB, Renard RA, Papadopoulos N, Gale NW, Thurston G, Yancopoulos GD, and Wiegand SJ. Delta-like ligand 4 (Dll4) is induced by VEGF as a negative regulator of angiogenic sprouting. *Proc Natl Acad Sci U S A* 104: 3219–3224, 2007.
38. Lough GC, Schauer JJ, Park JS, Shafer MM, Deminter JT, and Weinstein JP. Emissions of metals associated with motor vehicle roadways. *Environ Sci Technol* 39: 826–836, 2005.
39. MacKenzie F, Duriez P, Wong F, Noseda M, and Karsan A. Notch4 inhibits endothelial apoptosis via RBP-Jkappa-dependent and -independent pathways. *J Biol Chem* 279: 11657–11663, 2004.
40. McCreanor J, Cullinan P, Nieuwenhuijsen MJ, Stewart-Evans J, Malliarou E, Jarup L, Harrington R, Svartengren M, Han IK, Ohman-Strickland P, Chung KF, and Zhang J. Respiratory effects of exposure to diesel traffic in persons with asthma. *N Engl J Med* 357: 2348–2358, 2007.
41. Minicucci MF, Azevedo PS, Paiva SA, and Zornoff LA. Cardiovascular remodeling induced by passive smoking. *Inflamm Allergy Drug Targets* 8: 334–339, 2009.
42. Misra C, Kim S, Shen S, and Sioutas C. A high flow rate, very low pressure drop impactor for inertial separation of ultrafine from accumulation mode particles. *J Aerosol Sci* 33: 735–752, 2002.
43. Nel A, Xia T, Madler L, and Li N. Toxic potential of materials at the nanolevel. *Science* 311: 622–627, 2006.
44. Nemmar A, Hoet PHM, Vanquickenborne B, Dinsdale D, Thomeer M, Hoylaerts MF, Vanbilloen H, Mortelmans L, and Nemery B. Passage of inhaled particles into the blood circulation in humans. *Circulation* 105: 411–414, 2002.
45. Ono K. microRNAs and cardiovascular remodeling. *Adv Exp Med Biol* 888: 197–213, 2015.
46. Ooi AT, Ram S, Kuo A, Gilbert JL, Yan W, Pellegrini M, Nickerson DW, Chatila TA, and Gomperts BN. Identification of an interleukin 13-induced epigenetic signature in allergic airway inflammation. *Am J Transl Res* 4: 219–228, 2012.
47. Pekkanen J, Peters A, Hoek G, Tiittanen P, Brunekreef B, de Hartog J, Heinrich J, Ibald-Mulli A, Kreyling WG, Lanki T, Timonen KL, and Vanninen E. Particulate air pollution and risk of ST-segment depression during repeated submaximal exercise tests among subjects with coronary heart disease: the Exposure and Risk Assessment for Fine and Ultrafine Particles in Ambient Air (ULTRA) study. *Circulation* 106: 933–938, 2002.
48. Pellegrinet L, Rodilla V, Liu Z, Chen S, Koch U, Espinosa L, Kaestner KH, Kopan R, Lewis J, and Radtke F. Dll1- and dll4-mediated notch signaling are required for homeostasis of intestinal stem cells. *Gastroenterology* 140: 1230–1240.e1–e7, 2011.
49. Peters A, Wichmann HE, Tuch T, Heinrich J, and Heyder J. Respiratory effects are associated with the number of ultrafine particles. *Am J Respir Crit Care Med* 155: 1376–1383, 1997.
50. Pope CA, 3rd, Burnett RT, Thurston GD, Thun MJ, Calle EE, Krewski D, and Godleski JJ. Cardiovascular mortality and long-term exposure to particulate air pollution: epidemiological evidence of general pathophysiological pathways of disease. *Circulation* 109: 71–77, 2004.
51. Quillard T, Coupel S, Coulon F, Fitau J, Chatelais M, Cuturi MC, Chiffoleau E, and Charreau B. Impaired Notch4 activity elicits endothelial cell activation and apoptosis: implication for transplant arteriosclerosis. *Arterioscler Thromb Vasc Biol* 28: 2258–2265, 2008.
52. Ritz B, Yu F, Fruin S, Chapa G, Shaw GM, and Harris JA. Ambient air pollution and risk of birth defects in Southern California. *Am J Epidemiol* 155: 17–25, 2002.
53. Rodosthenous RS, Coull BA, Lu Q, Vokonas PS, Schwartz JD, and Baccarelli AA. Ambient particulate matter and microRNAs in extracellular vesicles: a pilot study of older individuals. *Part Fibre Toxicol* 13: 13, 2016.
54. Rostama B, Peterson SM, Vary CP, and Liaw L. Notch signal integration in the vasculature during remodeling. *Vascul Pharmacol* 63: 97–104, 2014.
55. Sardar SB, Fine PM, Mayo PR, and Sioutas C. Size-fractionated measurements of ambient ultrafine particle chemical composition in Los Angeles using the Nano-MOUDI. *Environ Sci Technol* 39: 932–944, 2005.
56. Schulz H, Harder V, Ibald-Mulli A, Khandoga A, Koenig W, Krombach F, Radykewicz R, Stampfl A, Thorand B, and Peters A. Cardiovascular effects of fine and ultrafine particles. *J Aerosol Med* 18: 1–22, 2005.
57. Stanger BZ, Datar R, Murtaugh LC, and Melton DA. Direct regulation of intestinal fate by Notch. *Proc Natl Acad Sci U S A* 102: 12443–12448, 2005.
58. Stone EA, Hedman CJ, Sheesley RJ, Shafer MM, and Schauer JJ. Investigating the chemical nature of humic-like substances (HULIS) in North American atmospheric aerosols by liquid chromatography tandem mass spectrometry. *Atmos Environt* 43: 4205–4213, 2009.
59. Takabe W, Li R, Ai L, Yu F, Berliner JA, and Hsiai TK. Oxidized low-density lipoprotein-activated c-Jun NH2-terminal kinase regulates manganese superoxide dismutase ubiquitination: implication for mitochondrial redox status and apoptosis. *Arterioscler Thromb Vasc Biol* 30: 436–441, 2010.
60. Verma V, Polidori A, Schauer JJ, Shafer MM, Cassee FR, and Sioutas C. Physicochemical and toxicological profiles of particulate matter in Los Angeles during the October 2007 southern California wildfires. *Environ Sci Technol* 43: 954–960, 2009.
61. Walshe TE, Connell P, Cryan L, Ferguson G, Gardiner T, Morrow D, Redmond EM, O'Brien C, and Cahill PA. Microvascular retinal endothelial and pericyte cell apoptosis in vitro: role of hedgehog and Notch signaling. *Invest Ophthalmol Vis Sci* 52: 4472–4483, 2011.
62. Wilhelm K, Happel K, Eelen G, Schoors S, Oellerich MF, Lim R, Zimmermann B, Aspalter IM, Franco CA, Boettger T, Braun T, Fruttiger M, Rajewsky K, Keller C, Bruning JC, Gerhardt H, Carmeliet P, and Potente M. FOXO1 couples metabolic activity and growth state in the vascular endothelium. *Nature* 529: 216–220, 2016.
63. Wu L, Li H, Jia CY, Cheng W, Yu M, Peng M, Zhu Y, Zhao Q, Dong YW, Shao K, Wu A, and Wu XZ. MicroRNA-223 regulates FOXO1 expression and cell proliferation. *FEBS Lett* 586: 1038–1043, 2012.
64. Yang L, Hou XY, Wei Y, Thai P, and Chai F. Biomarkers of the health outcomes associated with ambient particulate matter exposure. *Sci Total Environ* 579: 1446–1459, 2017.

65. Yu B, Zhou S, Wang Y, Qian T, Ding G, Ding F, and Gu X. miR-221 and miR-222 promote Schwann cell proliferation and migration by targeting LASS2 after sciatic nerve injury. *J Cell Sci* 125: 2675–2683, 2012.
66. Zhang Y, Schauer JJ, Shafer MM, Hannigan MP, and Dutton SJ. Source apportionment of in vitro reactive oxygen species bioassay activity from atmospheric particulate matter. *Environ Sci Technol* 42: 7502–7509, 2008.
67. Zhao M, Luo R, Liu Y, Gao L, Fu Z, Fu Q, Luo X, Chen Y, Deng X, Liang Z, Li X, Cheng C, Liu Z, and Fang W. miR-3188 regulates nasopharyngeal carcinoma proliferation and chemosensitivity through a FOXO1-modulated positive feedback loop with mTOR-p-PI3K/AKT-c-JUN. *Nat Commun* 7: 11309, 2016.

Address correspondence to:
Prof. Tzung K. Hsiai
Division of Cardiology
Department of Medicine
University of California, Los Angeles
10833 Le Conte Ave., CHS17-054A
Los Angeles, CA 90095-1679

E-mail: thsiai@mednet.ucla.edu

Date of first submission to ARS Central, May 14, 2017; date of acceptance, October 15, 2017.

Abbreviations Used

3D = three-dimensional
ADAM10 = a disintegrin and metalloproteinase domain-containing protein 10
BSA = bovine serum albumin
cDNA = complementary DNA
DA = dorsal aorta
DLAV = dorsal longitudinal anastomotic vessel
DN = dominant negative
dpa = days post-amputation
dpf = days post-fertilization
FBS = fetal bovine serum
FOXO = forkhead box O-subfamily
HAECs = human aortic endothelial cells
MAML1 = Master-mind like 1
miRNA = microRNA
MO = morpholino oligonucleotide
mRNA = messenger RNA
NICD = notch intracellular cytoplasmic domain
PCR = polymerase chain reaction
PFA = paraformaldehyde
PM = particulate matter
Rbp-Jκ = recombination signal-binding protein for immunoglobulin J region
siRNA = small interfering RNA
UFP = ultrafine particles
WT = wild type